nature nanotechnology

LETTERS

PUBLISHED ONLINE: 15 DECEMBER 2013 | DOI: 10.1038/NNANO.2013.265

Propagation of magnetic vortices using nanocontacts as tunable attractors

M. Manfrini[1,2], Joo-Von Kim[3,4], S. Petit-Watelot[3,4†], W. Van Roy[1], L. Lagae[1,2], C. Chappert[3,4] and T. Devolder[3,4*]

Magnetic vortices in thin films are in-plane spiral spin configurations with a core in which the magnetization twists out of the film plane[1,2]. Vortices result from the competition between atomic-scale exchange forces and long-range dipolar interactions. They are often the ground state of magnetic dots[3,4], and have applications in medicine[5], microwave generation[6,7] and information storage[8]. The compact nature of the vortex core, which is 10–20 nm wide, makes it a suitable probe of magnetism at the nanoscale[9]. However, thus far the positioning of a vortex has been possible only in confined structures, which prevents its transport over large distances. Here we show that vortices can be propagated in an unconstrained system that comprises electrical nanocontacts (NCs). The NCs are used as tunable vortex attractors in a manner that resembles the propelling of space craft with gravitational slingshots. By passing current from the NCs to a ferromagnetic film, circulating magnetic fields are generated, which nucleate the vortex and create a potential well for it. The current becomes spin polarized in the film, and thereby drives the vortex into gyration through spin-transfer torques[10]. The vortex can be guided from one NC to another by tuning attractive strengths of the NCs. We anticipate that NC networks may be used as multiterminal sources of vortices and spin waves (as well as heat, spin and charge flows) to sense the fundamental interactions between physical objects and fluxes of the next-generation spintronic devices.

Magnetic vortices need strong dipolar confinement, and are usually studied in micro- or nanostructures. In extended films, vortices can be generated in the NC geometry[3,10] by passing a charge current into a magnetic multilayer through a metallic NC. The NC supplies energy to and causes attraction of the vortex because of spin-transfer torques and the Oersted field from the current, respectively. In this system, the vortex undergoes a stationary orbital motion (on a 100 nm scale) about the NC, which can be detected through time-dependent changes in the NC resistance[4,11]. The changes in vortex dynamics in the presence of forces supplied by several NCs are yet to be determined[12]. In particular, whether forces from multiple NCs can provide mobility to the vortices needs to be established. Here we show that proper partitioning of the currents among the NC attractors can be used to tailor the vortex trajectories and transport the vortices over large distances. We illustrate the controlled manipulation of vortices by channelling them back and forth in various NC chains.

We use metallic NCs (Fig. 1a) with a radius of 50 nm to route currents into an extended soft magnetic film that has uniform magnetization at remanence. The magnetic state is known from its magnetoresistance because of dynamically inactive reference layers underneath.

When a single NC is used, the current flowing through it results in an Oersted field that can trigger the nucleation of a vortex–antivortex pair, with the antivortex being expelled out of the region of interest[3,13]. At low currents (10–40 mA), the nucleated vortex remains in the vicinity of the NC by virtue of an attractive force that results from the Zeeman energy associated with the Oersted field. Consequently, the vortex spirals to a limit cycle at which magnetic damping is compensated by spin torques associated with spin-polarized currents that flow radially outwards from the NC in the film plane. The orbital revolution of the vortex about the NC leads to an electrical microwave signal in the subgigahertz range[4], where the frequency reflects the strength of the attractive force, which is proportional to the current[11].

To assess a broader range of dynamics, we prepared pair (Fig. 1b) and quadruple NC arrays, where the latter include lines, Y branches and diamond arrangements (Fig. 1c), with centre-to-centre NC separations that ranged from 300 nm to 1,500 nm. The electrode geometry ensures independent electrical access to each NC.

Two competing phenomena can be anticipated in systems with multiple NCs. Indeed, as a current passing through a single NC nucleates a vortex, it has been speculated that by distributing the current across several NCs one could create multiple vortices and antivortices to form an array that reflects the NC arrangement[12]. In a contrasting scenario, passing current in additional NCs induces additional forces, with the possible consequence of simply reorganizing the vortex orbit. To investigate this in more detail, we first studied a double NC system that comprised East and West NCs with a 500 nm separation (Fig. 1a). In a first experiment (Fig. 2a), we nucleated a vortex on the East NC with subsequent current conditions, written as $\{I_W, I_E\} = \{0, 20\}$ mA. The microwave voltage spectra (Fig. 2a) confirm that the vortex orbits about the East NC. Starting from this condition, we fixed the total current $I_W + I_E$ to 20 mA and gradually increased the current applied to the West NC. When the applied currents through the two NCs were approximately equal, a copy of the East power spectrum was detected on the West NC. The fundamental spectral lines recorded on the two NCs then have identical frequencies and linewidths, irrespective of the position of the initial vortex nucleation. The spectra only differ in their power partition among the harmonics. This very probably corresponds to two separate observations of the same oscillatory dynamics. When the gradual transfer of current towards the West NC was resumed, the signal disappeared gradually from East until the case where $\{I_W, I_E\} = \{20, 0\}$ mA, at which the vortex orbited solely about the West NC. The electrical signature of the vortex oscillation did not disappear during that shifting of the current. This suggests that a single vortex was transferred from an orbit

[1]IMEC, Kapeldreef 75, B-3001 Leuven, Belgium, [2]Laboratorium voor Vaste-Stoffysica en Magnetisme, Katholieke Universiteit Leuven, Celestijnenlaan 200 D, B-3001 Leuven, Belgium, [3]Institut d'Electronique Fondamentale, Centre National de la Recherche Scientifique, Unité Mixte de Recherche 8622, 91405 Orsay, France, [4]Université Paris-Sud, 91405 Orsay, France; †Present address: Institut Jean Lamour, Centre National de la Recherche Scientifique – Université de Lorraine, Boulevard des Aiguillettes BP 70239, F-54506 Vandoeuvre les Nancy, France. *e-mail: thibaut.devolder@u-psud.fr

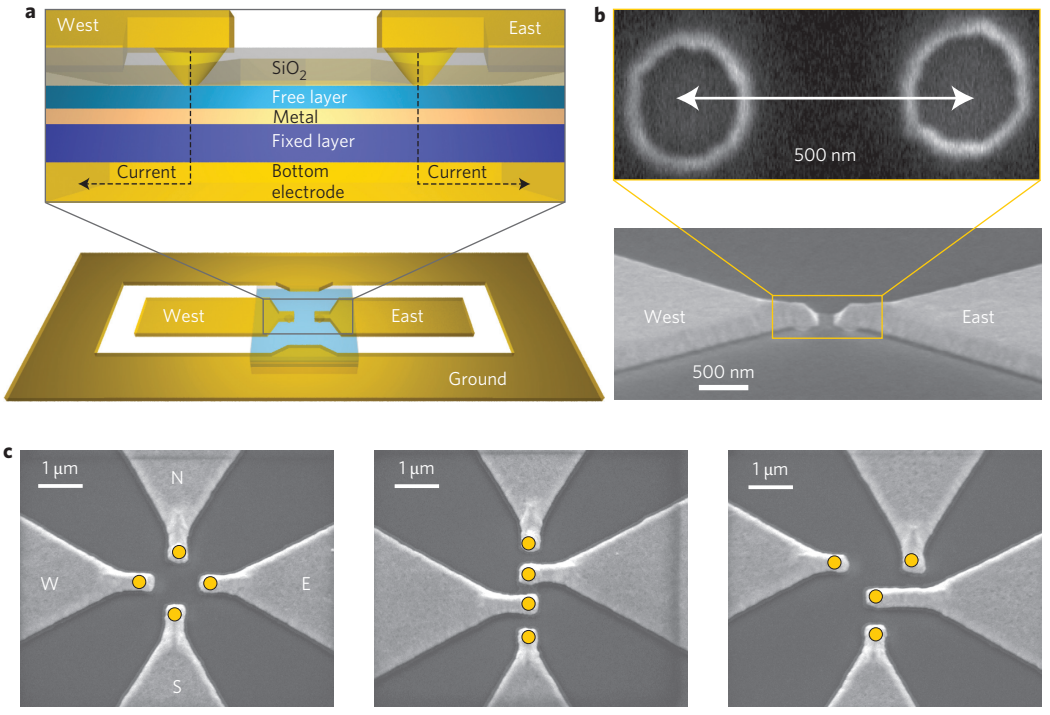

Figure 1 | Extended system with arrays of NCs. a, Sketch of two NCs fabricated on top of a spin valve consisting of a magnetically soft free layer stacked onto a metallic spacer and an exchanged bias, magnetically hard-pinned layer. **b**, Scanning electron microscopy images of the two NCs during (top) and after (bottom) microfabrication. **c**, Multiple NC arrangements (from left to right): diamond, four-item line and Y-shaped branching network. The yellow dots sketch the positions and sizes of the NCs.

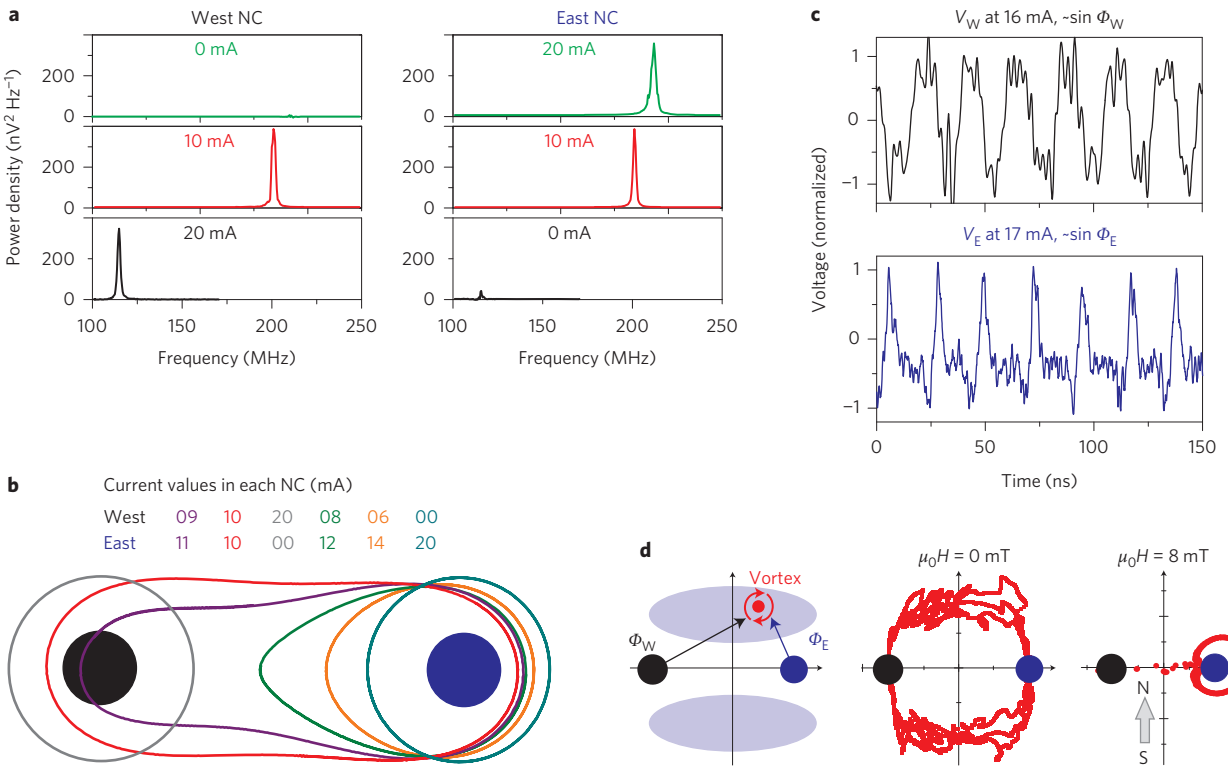

Figure 2 | Vortex transfer in a pair of 500-nm-spaced NCs. a, Voltage spectra recorded on each NC, just after nucleation on the East NC (green curves), at equal current sharing (red) and when routing all the current to the West NC (black). **b**, Micromagnetic simulation of the vortex trajectories during the current repartitioning procedure in **a**. **c**, Normalized time-resolved magnetoresistance of the two NCs in nearly equal current conditions, and no applied field (the angles Φ_W and Φ_E are sketched in **d**). **d**, Construction of the vortex trajectory of **c** by triangulation for two applied fields *H*. The light-grey area (left diagram) indicates qualitatively the region in which the triangulation is reliable. The middle diagram shows the raw-data trajectory during three turns in zero field. The right diagram is the event-averaged trajectory when applying a field that pushes the vortex towards East.

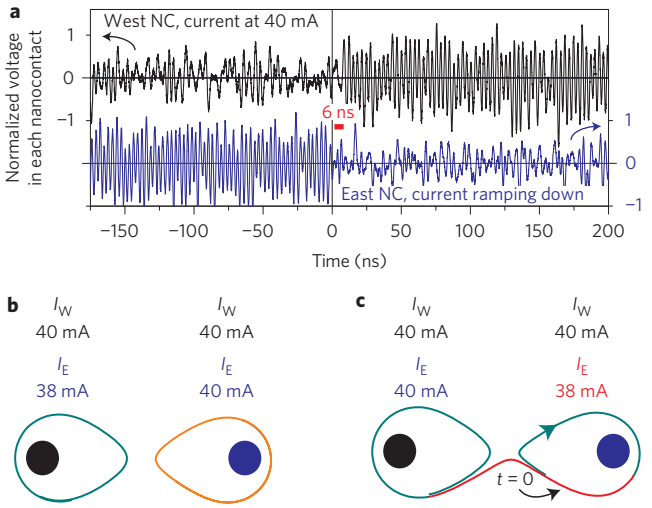

Figure 3 | Release and capture of a vortex in NCs separated by 680 nm. **a**, Experimental voltages recorded on the NC releasing the vortex (blue, 37 mA ramping down) and the NC capturing the vortex (black, fixed 40 mA current). **b**, Simulated steady-state orbits in asymmetric and symmetric current conditions. **c**, Simulated trajectory after an abrupt change from symmetric to asymmetric current conditions. The colour changes every 4 ns.

about the initial NC to an orbit that passes near, intercepts or encompasses both NCs.

To shed light on the transfer mechanism we simulated the vortex dynamics during this current-shifting procedure (Fig. 2b). We considered the two NCs in a defect-free magnetic layer (see Methods). The simulation began with a circular vortex orbit about the East NC. As the current is reduced gradually in the East NC and increased in the West NC, the minimum in the Zeeman energy potential experienced by the vortex gradually shifts towards the West NC, which results in a distortion in the orbit (Fig. 2b and Supplementary Video 3). In the cases where the applied currents through the two NCs are almost equal ($9 \leq I_W \leq 11$ mA), the potential minimum shifts towards the midpoint between the two NCs and the orbit encompasses the two NCs (Supplementary Video 4). As the current is further increased in the West NC, the vortex is released from the East NC and orbits exclusively around the West NC.

When the vortex undergoes a trajectory that encompasses the two NCs, the phases Φ_W and Φ_E of time-resolved resistance signals recorded on each NC differ (Fig. 2c). These phases are essentially the azimuthal directions under which each NC 'sees' the vortex, such that their measurement allows us to obtain the vortex position by a crude form of triangulation (Fig. 2d). As for any triangulation performed with only two observers, it can be done only when the vortex is not located along the line that joins the two NCs (that is, $\Phi_E \approx 0$). In addition, even if higher currents are used to improve the accuracy of the phase measurement, the electrical noise levels make triangulation unreliable when $\Phi_W \approx \Phi_E$ (that is, when the vortex is too far away). However, in the region of reliable triangulation, the orbit obtained in zero field is consistent with a vortex trajectory that encompasses both NCs. We can suppress the encompassing character of the vortex orbit by applying a magnetic field oriented to the North, which creates a force that pushes the vortex towards East. In this case, the West voltage decreases substantially and its frequency doubles. Real-time triangulation cannot be done at this low level of signal. Nevertheless, an averaging procedure allows us to visualize the mean vortex trajectory, which is now about East (Fig. 2d).

A different behaviour appears for larger NC separations. At a separation of 680 nm, the vortex trajectories are not observed to encompass the two NCs. The transfer requires not only substantially higher currents, but also an asymmetric partitioning. Let us describe one of the working protocols. We start at $\{I_W, I_E\} = \{40, 0\}$ mA with a vortex on West. Ramping up the East current until {40, 40} mA does not significantly affect the voltage powers measured at each NC. To transfer the vortex, we need to weaken the attraction of the West NC by ramping down its current. At {38, 40} mA, the vortex is released from West: the vortex gyration signal disappears from the West NC and appears on the East NC (Fig. 3). This contrasts with the previous case of smaller (500 nm) separation (Fig. 2), where the signal shifted gradually between the NCs.

To obtain more insight into this process, we monitored it in real time. There was some variability in the transfer dynamics. In most instances (Fig. 3a), the oscillatory signal on the destination NC starts a few nanoseconds after the termination of the oscillation on the

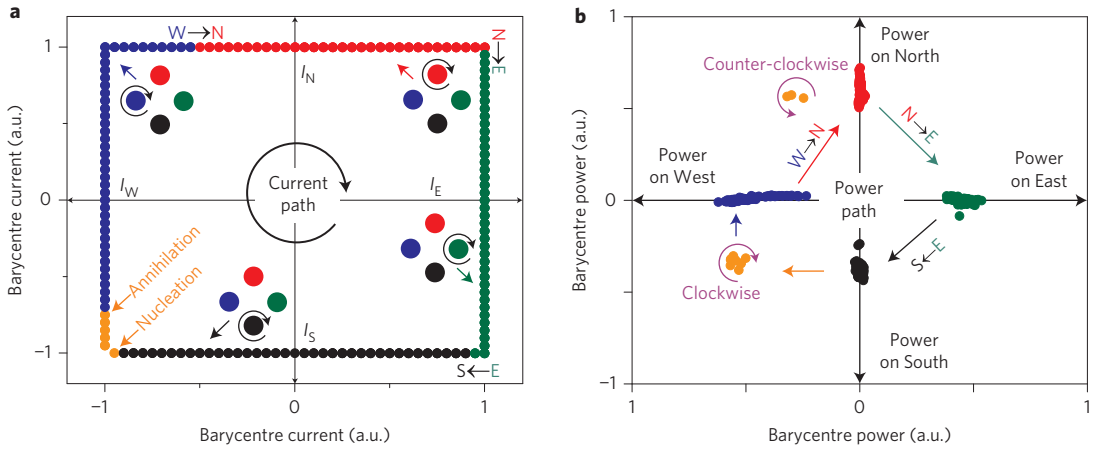

Figure 4 | Vortex shifting in a network of four NCs placed in a diamond arrangement (Fig. 1c, left). **a**, Current-shifting path for a clockwise guiding of the vortex. The symbol coordinates are constructed by allocating weights of (1, 0), (0, 1), (−1, 0) and (0, −1) to North (N), East (E), South (S) and West (W) currents after a normalization by 40 mA. The currents are always positive. The sketches and the symbol colours were chosen to illustrate the NC about which the vortex is orbiting. **b**, The resulting shifting of the voltage power. The symbol positions were constructed by allocating weights of (1, 0), (0, 1), (−1, 0) and (0, −1) to North, East, South and West powers after a normalization by 1 nW. The arrows denote the vortex hopping, the nucleation of a second vortex or its annihilation. The orange symbols correspond to states with two vortices with corresponding spectra similar to those in Supplementary Fig. 2. a.u., arbitrary units.

departure NC. Once released, the vortex is captured and immediately starts to orbit about the destination NC—the vortex trajectory 'hops' from one attractor to another. In the other cases (Supplementary Fig. 1), there is an intermediate microwave quiet state during the transfer. The lifetime of this state varies between zero and a few microseconds in a manner consistent with an Arrhenius process.

One may wonder why the transfer of vortices is so dependent on the NC separation. To elucidate this point, we simulated the dynamics with a large NC separation (Fig. 3b). In this geometry, a balanced sharing of the current does not yield an encompassing trajectory—at equal currents, the vortex orbits about a single NC and it keeps away from the midpoint of the two NCs (Fig. 3b). The simulation also confirms that the transfer happens only when the attraction of the departure NC is reduced, which explains the hysteretic character of the transfer. For the defect-free sample, the rotation about the destination NC is predicted to follow the release immediately. During the transfer, the vortex approaches the midway point between the two NCs, where its linear velocity substantially decreases. In this region the two attractors compete: the total Oersted field vanishes, which leads to a minimum of the Zeeman potential energy of the vortex. In addition, the spin torque that acts on the vortex vanishes because the currents from the two NCs cancel out in this region. These two facts lead to a slowing down of the vortex, which may be responsible for the two-step transfer events seen experimentally. Indeed, we suspect that during this stochastic delay the vortex can be pinned at some defect between the two NCs. In fact, the localized character of the vortex core makes it prone to pinning[14]. A transient pinning scenario is further supported by complementary studies in which we varied the free-layer composition to increase its pinning ability (Supplementary Fig. 1).

Finally, to show that we can controllably propagate the vortex back and forth over micron-length scales, we used more-complex geometries, such as the chains and branching displayed in Fig. 1c. When using, for instance, a diamond arrangement of NCs placed at the four cardinal points, North, East, South and West, we can transfer the vortex from one cardinal point to the next (Fig. 4). We used the hopping protocol, described previously (Fig. 3), by cycling the current in a clockwise manner. Starting with a vortex that orbits about the North NC, with $\{I_N, I_E, I_S, I_W\} = \{40, 0, 0, 0\}$ mA, we ramped the East current until we reached {40, 40, 0, 0} mA. At this current combination, the vortex still orbits about North. Then, ramping the North current down to {38, 40, 0, 0} mA makes the vortex hop to East. This process was repeated to guide the vortex to any NC of the diamond NC arrangement (Fig. 4). The vortex transfer requires a higher current in the capturing NC than that of the releasing NC, except when the NCs have substantially different sizes (Supplementary Fig. 2). This protocol can be repeated along any chain of closely separated NCs to propagate controllably a single vortex over micrometre-length scales.

In summary, we have demonstrated the manipulation of vortex trajectories in networks of NCs that act as tunable attractors. This reveals the possibility of controllably propagating vortices over micron-length scales in extended films, which is unexpected given their inherent gyrotropic properties. This is in stark contrast to well-reported vortex gyration in magnetic dots, in which vortices are confined and gyration radii can be, at most, of the order of 100 nm. As a vortex is both a well-defined nanoscale magnetization gradient and its trajectory can be adjusted to become very sensitive to external perturbations, it could be used as an accurate probe to understand novel effects, such as, for instance, spin caloritronics[15], in situations that may become generic of advanced spintronic devices. Indeed, a NC network may be used as a multiterminal source of vortices, heat flow[16], spin flow[17], charge flow and spin-wave flow[18,19] to provoke and sense interactions between these physical objects.

Methods

Samples. The experiments were conducted on spin valves with a free layer of composition $Co_{90}Fe_{10}$ (1.5 nm)/$Ni_{80}Fe_{20}$ (2 nm). A small (0.7 mT) uniaxial anisotropy was obtained by annealing under applied fields, which ensures uniform magnetization at remanence. A 0.3% magnetoresistance was provided by the magnetic layers underneath. They included a pinned layer of composition $Ir_{22}Mn_{78}$ (8 nm)/$Co_{90}Fe_{10}$ (3 nm). The metallic spacer was 2.3 nm of copper. Our NCs were made of gold. Their base radius was 50 nm and shaped like an inverted truncated cone[20]. Vortex nucleation was performed with intense (60 mA), short (10 ns) current pulses.

Additional experiments were performed on samples with a pseudo spin-valve structure, of composition Au (30 nm)/Co (10 nm)/Au (5 nm)/Co (5 nm)/Pt (4 nm). With these samples, the absence of exchange bias yielded a reduced usable current interval, combined with a higher pinning effect that manifested in a larger coercivity of the cobalt-free layer. In cobalt-based pseudospin valves, the transfer of vortices in linear chains of NCs spaced by 500 nm systematically involved vortex pinning, with either the two-step scenario of Supplementary Fig. 1 or a finite current interval in which the vortex signal was lost in between two successive NCs.

Micromagnetic simulation method. For the micromagnetic simulations shown in Figs 2 and 4, we used the micromagnetic simulation package MuMax[21]. The magnetic field and current lines are computed by finite element simulations with the real layer stack and NC profiles, in a similar way to Petit-Watelot *et al.*[20]. The in-plane current provides the sole source of spin torque, with the spin polarization of the current assumed to be 50%. The simulations were performed on stadium-shaped areas of $2.56 \times 1.28\ \mu m^2$ (see, for instance, Supplementary Video 4), which proved much larger than the area in which magnetization dynamics occurs. We let the simulations run for at least 100 ns, which is longer than the steady-state orbital periods (3–20 ns, depending on the applied currents) and longer than the time required to reach the limit-cycle orbits. In the worst case (a two-NC system with balanced or nearly balanced currents), five periods were needed to reach within 5 nm distance of the limit cycle.

Measurement methods. In the time-resolved measurement of the vortex hopping presented in Fig. 3, each NC voltage, $V_W(t)$ and $V_E(t)$ were connected to the input channels of a Lecroy SDA 18000 single-shot oscilloscope. The bandwidth of the measurement chains were Gaussian with a roll-off of 350 MHz and a d.c. cut-off of 10 MHz, set to both maximize the signal-to-noise ratio and avoid distortion of the voltage waveforms. The amplifiers and the filters in the two signal transmission chains were balanced carefully to ensure that the measurements of the two NCs were done with the same time origin, within a few nanoseconds.

In the triangulation method of the encompassing trajectory (Fig. 2d), each of the two NC voltages was first transformed into a time-resolved, normalized magnetoresistance signal. The normalization required an exact determination of the peak-to-peak amplitudes of the two signals, which was performed by deconvoluting the measurement-system Gaussian noise from the voltage probability distribution of each time trace. For triangulation, we needed an absolute de-skewing of the time axes, because any error in the estimation of the phases results in a dramatically incorrect vortex position. The correction of the intertrace delay was performed mathematically by maximizing the intertrace intercorrelation product at zero delay. This is rigorous if the two signals are two observations of the same dynamics that possess identical phase noise described by a single relaxation time[13,22]. Once synchronized, the curves were smoothed using the quadratic Savitzky–Golay algorithm, with an aperture compatible with the signal bandwidth. The phases Φ_W and Φ_E were deduced from the argument of the analytical signal obtained by combining the signals with their Hilbert transform, following Bianchini *et al.*[23]. Finally, triangulation was performed by assuming that the micromagnetic texture was determined only by the vortex core position, and that the vortex profile was not distorted compared to a vortex at remanence in an ultrathin film.

In the triangulation method for the vortex mean trajectory in 8 mT of applied field, there were two main differences. First, we performed averaging on the oscilloscope, with a trigger criterion on the high-amplitude East signal. Second, the low-amplitude West signal was bandpass filtered around its main frequency line, which was at twice the frequency of the East signal. The d.c. offset of the West signal was added mathematically before deducing $\sin(\Phi_W)$ by a simple inverse cosine function.

Received 21 June 2013; accepted 8 November 2013; published online 15 December 2013

References

1. Shinjo, T., Okuno, T., Hassdorf, R., Shigeto, K., Ono, T. Magnetic vortex core observation in circular dots of permalloy. *Science* **289,** 930–932 (2000).
2. Tretiakov, O. A. & Tchernyshyov, O. Vortices in thin ferromagnetic films and the skyrmion number. *Phys. Rev. B* **75,** 012408 (2007).
3. Mistral, Q. *et al.* Current-driven vortex oscillations in metallic nanocontacts. *Phys. Rev. Lett.* **100,** 257201 (2008).

4. Petit-Watelot, S. *et al.* Commensurability and chaos in magnetic vortex oscillations. *Nature Phys.* **8,** 682–687 (2012).
5. Kim, D-H. *et al.* Biofunctionalized magnetic-vortex microdiscs for targeted cancer-cell destruction. *Nature Mater.* **9,** 165–171 (2010).
6. Pribiag, V. S. *et al.* Magnetic vortex oscillator driven by d.c. spin-polarized current. *Nature Phys.* **3,** 498–503 (2007).
7. Jain, S. *et al.* From chaos to selective ordering of vortex cores in interacting mesomagnets. *Nature Commun.* **3,** 1330 (2012).
8. Yu, Y-S. *et al.* Memory-bit selection and recording by rotating fields in vortex-core cross-point architecture. *Appl. Phys. Lett.* **98,** 052507 (2011).
9. Burgess, J. A. J. *et al.* Quantitative magneto-mechanical detection and control of the Barkhausen effect. *Science* **339,** 1051–1054 (2013).
10. Kasai, S., Nakatani, Y., Kobayashi, K., Kohno, H. & Ono, T. Current-driven resonant excitation of magnetic vortices. *Phys. Rev. Lett.* **97,** 107204 (2006).
11. Devolder, T. *et al.* Time-resolved zero field vortex oscillations in point contacts. *Appl. Phys. Lett.* **95,** 012507 (2009).
12. Ruotolo, A. *et al.* Phase-locking of magnetic vortices mediated by antivortices. *Nature Nanotech.* **4,** 528–532 (2009).
13. Devolder, T. *et al.* Vortex nucleation in spin-torque nanocontact oscillators. *Appl. Phys. Lett.* **97,** 072512 (2010).
14. Compton, R. L. & Crowell, P. A. Dynamics of a pinned magnetic vortex. *Phys. Rev. Lett.* **97,** 137202 (2006).
15. Bauer, G. E. W., Saitoh, E. & van Wees, B. J. Spin caloritronics. *Nature Mater.* **11,** 391–399 (2012).
16. Petit-Watelot, S. *et al.* Understanding nanoscale temperature gradients in magnetic nanocontacts. *Phys. Rev. Lett.* **109,** 267205 (2012).
17. Jedema, F. J., Filip, A. T. & van Wees, B. J. Electrical spin injection and accumulation at room temperature in an all-metal mesoscopic spin valve. *Nature* **410,** 345–348 (2001).
18. Kaka, S. *et al.* Mutual phase-locking of microwave spin torque nano-oscillators. *Nature* **437,** 389–392 (2005).
19. Madami, M. *et al.* Direct observation of a propagating spin wave induced by spin-transfer torque. *Nature Nanotech.* **6,** 635–638 (2011).
20. Petit-Watelot, S., Otxoa, R. M. & Manfrini, M. Electrical properties of magnetic nanocontact devices computed using finite-element simulations. *Appl. Phys. Lett.* **100,** 083507 (2012).
21. Vansteenkiste, A. & Van de Wiele, B. MuMax: a new high-performance micromagnetic simulation tool. *J. Magn. Magn. Mater.* **323,** 2585–2591 (2011).
22. Keller, M. W., Kos, A. B., Silva, T. J., Rippard, W. H. & Pufall, M. R. Time domain measurement of phase noise in a spin torque oscillator. *Appl. Phys. Lett.* **94,** 193105 (2009).
23. Bianchini, L. *et al.* Direct experimental measurement of phase-amplitude coupling in spin torque oscillators. *Appl. Phys. Lett.* **97,** 032502 (2010).

Acknowledgements

M.M. acknowledges J. Moonens for e-beam lithography and J. Loo and P. Neutens for scanning electron microscopy images. J-V.K., S.P.W., C.C. and T.D. acknowledge support from an the French National Research Agency through contract no. ANR-09-NANO-006 (VOICE).

Author contributions

J-V.K., M.M. and T.D. conceived the experiment. M.M. designed and fabricated the samples. W.v.R. and L.L. supervised the device integration. T.D. and C.C. developed the high-frequency setup. M.M. and T.D. performed the measurements. S.P-W. calculated the current and field distributions. J-V.K. performed the analytical and micromagnetic modelling. T.D., M.M. and J-V.K. analysed and interpreted the data. J-V.K., M.M. and T.D. prepared the manuscript. All authors commented on the manuscript.

Additional information

Supplementary information is available in the online version of the paper. Reprints and permissions information is available online at www.nature.com/reprints. Correspondence and requests for materials should be addressed to T.D.

Competing financial interests

The authors declare no competing financial interests.